Assessment of ERS synthetic aperture radar wave spectra retrieved from the Max-Planck-Institut (MPI) scheme through intercomparisons of 1 year of directional buoy measurements

N. Violante-Carvalho
Department of Oceanography, Rio de Janeiro State University, Rio de Janeiro, Brazil

I. S. Robinson
Southampton Oceanography Centre, University of Southampton, Southampton, UK

J. Schulz-Stellenfleth
Institut für Methodik der Fernerkundung, Deutschen Zentrum für Luft-und Raumfahrt, Wessling, Germany

Received 13 March 2004; revised 21 March 2005; accepted 25 April 2005; published 26 July 2005.

[1] One year of directional buoy measurements comprising the period from May 1994 to April 1995 acquired in deep ocean waters by an offshore heave-pitch-roll buoy are used for the assessment of the directional wave spectra retrieved from synthetic aperture radar (SAR) images using the Max-Planck-Institut (MPI) scheme. SAR is the only sensor so far deployed from satellites that can provide measurements of the directional wave spectrum with high spatial and temporal coverage when operating in the so-called SAR wave mode. Millions of SAR wave mode imagettes have been and are still being acquired over all oceanic basins yielding a powerful data set for investigating wind waves. However, directional spectral information retrieved from SAR images has not yet been assessed against in situ measurements. For the first time, detailed validations of the main wave parameters, that is, significant wave height, mean direction of propagation, and mean wavelength, are performed. It is shown that in terms of these parameters the first-guess spectra taken from the wave model WAM are in better agreement with the buoy measurements than the MPI scheme retrievals. When considering only the longer waves in the part of the spectrum observed by SAR, on the other hand, the algorithm performs at least as well as the third-generation WAM wave model. In addition to the limitations of the MPI scheme in extending the spectral information beyond the high wave number cut-off, an observed misinterpretation of wind sea energy as swell by the MPI scheme is shown to be caused by the use of a quasi-linear approximation of the imaging model in the numerical iteration procedure.

Citation: Violante-Carvalho, N., I. S. Robinson, and J. Schulz-Stellenfleth (2005), Assessment of ERS synthetic aperture radar wave spectra retrieved from the Max-Planck-Institut (MPI) scheme through intercomparisons of 1 year of directional buoy measurements, *J. Geophys. Res.*, *110*, C07019, doi:10.1029/2004JC002382.

1. Introduction

[2] The launch of the first European Remote Sensing Satellite (ERS-1) in 1991 was a turning point for the continuous observation of the detailed spectral properties of ocean wind waves and for the investigation of their climatology. For the first time the two-dimensional directional wave spectrum became available with high spatial and temporal coverage over all oceanic basins through the wave mode of the synthetic aperture radar (SAR). With the subsequent launch of its successors ERS-2 and ENVISAT, over 10 years of global measurements and millions of SAR wave mode (SWM) imagettes have been and are still being acquired in quasi-real time, yielding a unique opportunity for the improvement of our understanding of the mechanisms that govern the growth and evolution of waves.

[3] The potentialities of these data are enormous. The better estimation through numerical simulations of the wave field using past forcing winds to compute the climatologies (hindcasts) or for wave forecasts has practical importance for activities such as for ship routing, offshore engineering, coastal management, and fisheries. To achieve improvements, wave models have to rely on detailed spectral measurements which are available, with adequate spatial and temporal coverage, only from sensors onboard satellites.

0148-0227/05/2004JC002382$09.00

[4] Advances in our understanding of surface wave processes translating into better estimates through numerical simulations will necessarily require improvements in satellite remote sensing retrievals and more comprehensive schemes for the assimilation of this information into wave models. Present operational methods are still based on the relatively simple optimal interpolation schemes [*Lionello et al.*, 1992; *Hasselmann et al.*, 1997; *Voorrips et al.*, 1997]. So far, only significant wave heights (SWH) obtained from altimeters have been assimilated operationally into wave models. However, despite its positive impact on forecasts, the use of an integral parameter such as SWH still has limitations since the averaged energy has to be distributed somehow over the entire spectrum. The use of more sophisticated methods (such as the Green's Function Method proposed by *Bauer et al.* [1996]) that take advantage of the detailed spectral information yielded by SAR have not yet been implemented operationally but have already shown the potentialities of the technique. Variational methods are able to track swell component back in time and space and so correct the forcing wind at a time preceding the available observations, promising better forecasts in coupled atmosphere-ocean models. More advanced spectrum assimilation methods using the adjoint technique and the Kalman filter should be further explored although their feasibility has already been demonstrated [*de las Heras et al.*, 1994; *Voorrips et al.*, 1999].

[5] The retrieval of the directional wave spectrum from SAR images is not, however, a trivial exercise. There are two main limitations in the SAR ocean wave imaging mechanisms. First, there is a 180° directional ambiguity observed in frozen images. This problem has been solved with the launch of ENVISAT carrying the Advanced Synthetic Aperture Radar (ASAR) which computes two successive images resolving the propagation direction. Second, the SAR imaging mechanism is strongly nonlinear owing to the vertical orbital movements induced by the waves which causes a Doppler offset in the image plane with smearing and loss of information beyond a high wave number cut-off. These limitations require the use of additional information, in general a first guess wave spectrum from a model, to solve the ambiguity and to augment the spectral information in the high wave number part of the spectrum.

[6] The problem of directional ambiguity and lack of information beyond a high wave number cut-off has been tackled by three different methods. The basic difference in their strategies lies in how they address the problem of reconstructing the directional spectrum beyond the high wave number azimuthal cut-off and hence filling in the spectral gap in the wind sea part of the spectrum [*Hasselmann and Hasselmann*, 1991; *Hasselmann et al.*, 1996; *Krogstad et al.*, 1994; *Mastenbroek and de Valk*, 2000].

[7] The first retrieval algorithm was developed at the Max-Planck-Institut (MPI) by *Hasselmann and Hasselmann* [1991], and an improved version was presented later [*Hasselmann et al.*, 1996]. They proposed an expression for the mapping of a wave spectrum onto a SAR image spectrum together with a technique to invert the mapping relation. The second retrieval scheme to be proposed [*Krogstad et al.*, 1994] is a simplified version of the MPI scheme which uses a quasi-linear approximation of Hasselmann and Hasselamann's full nonlinear forward mapping relation. The Semi-Parametric Retrieval Algorithm (SPRA) [*Mastenbroek and de Valk*, 2000], the third retrieval scheme, employs the wind information from the scatterometer that is operating simultaneously with the SAR. Therefore there is no need for a first guess from a wave model since they apply a parameterized wind sea spectrum. In this work we will discuss the performance of the MPI retrieval scheme. For more details about the MPI scheme see *Hasselmann and Hasselmann* [1991] and *Hasselmann et al.* [1996]; a revision of the main features of the SAR ocean wave imaging mechanisms together with a detailed description of the retrieval algorithm is presented by *Violante-Carvalho and Robinson* [2004].

[8] *Voorrips et al.* [2001] (hereinafter referred to as VMH01) compared the MPI and the SPRA schemes against several nondirectional buoys deployed mostly off the North American coast. In that work it became clear that both schemes have room for improvement, and that their main deficiencies lie in how to augment the spectral information beyond the azimuthal cut-off. However, one of the most striking characteristics of SAR data, its directional spectral information, was not considered. The main problem for such a comparison is a lack of available directional buoy data in deep water. The few directional buoys available to VMH01 were not included in their analysis because they are moored in relatively shallow coastal waters, where one would expect a greater spatial variation of the wave parameters when compared to the more spatially homogeneous situations in the open sea. The present work aims to validate the MPI retrieval scheme using for the first time directional wave data from a heave-pitch-roll buoy moored in deep water.

2. Collocated Data Set and Wave Data

2.1. Buoy Measurements

[9] Campos Basin, in the coast off Rio de Janeiro (Figure 1), is the most important petrolic basin in Brazil. Tens of platforms are located in this area responsible for over 75% of the oil produced by the country, with several offshore operations taking place daily. In addition, the surrounding area holds a high urban concentration with strong commercial and industrial activities. A heave-pitch-roll buoy was deployed during the period from March 1991 to March 1993 and from January 1994 to July 1995 at the position 22°31′S and 39°58′W in a depth over 1000 m around 150 km offshore. Meteorological data (wind speed and direction, air temperature, and air pressure) as well as sea surface data (intensity and direction of currents, temperature, and salinity) were also acquired. The wave spectrum is calculated using classical Fourier analysis, and the spreading function is estimated using the Maximum Entropy Method [*Lygre and Krogstad*, 1986]. More details about the buoy and how the spectral analysis was performed are provided by *Violante-Carvalho et al.* [2004].

[10] This data set yields a unique opportunity to investigate the retrievals of wave spectra from SAR images. In the first place, directional buoy measurements in deep water are scarce. The buoys under the supervision of the National Oceanic and Atmospheric Administration (NOAA) are located mainly in relatively shallow waters and are almost

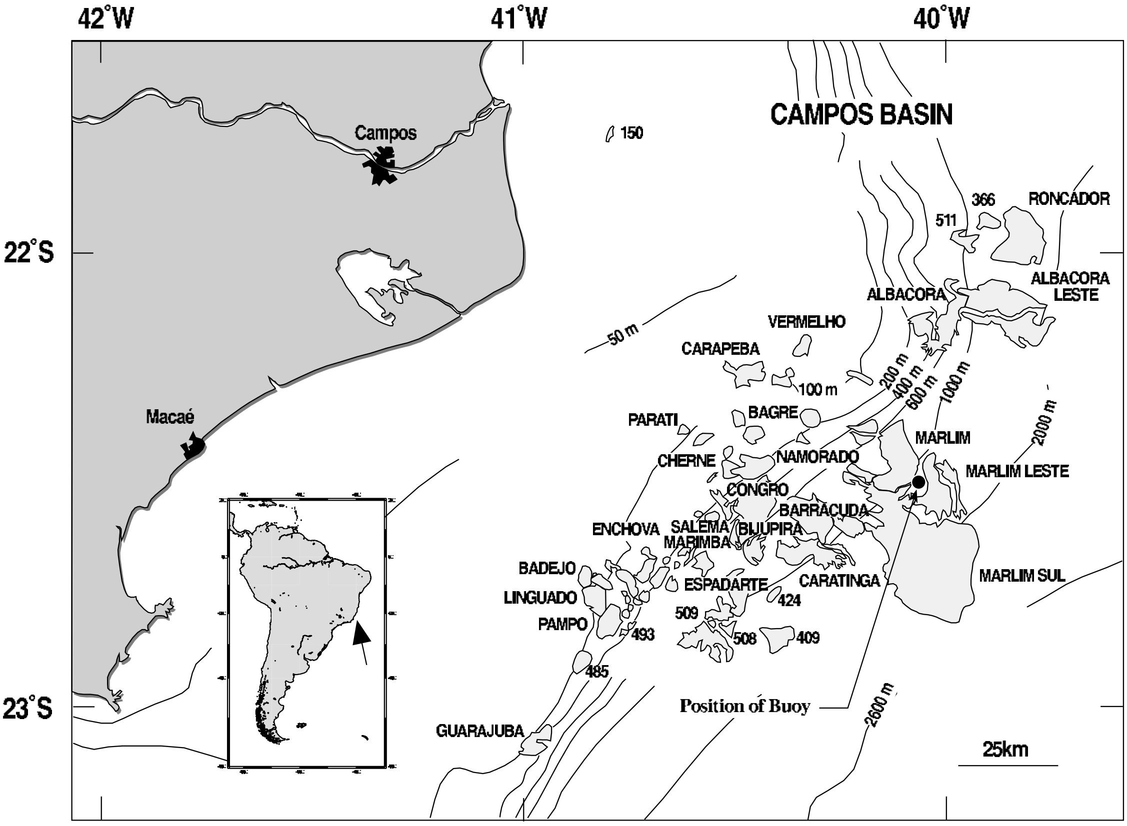

Figure 1. South Atlantic and position of the buoy in Campos Basin in the southeastern coast of Brazil. The shaded areas are the oil fields.

all omni-directional. The location of buoys in shallow waters introduces an additional complication to any sort of analysis due to the spatially high gradients of the wave parameters compared to the more homogeneous situations encountered in the open ocean. The other well-known source of wave measurements is the network deployed in relatively shallow waters in the North Sea which are, in their majority, directional buoys. Nevertheless, when passing over this region the ERS SAR is often switched to image mode which yielded only a few SWM imagettes during the several years of SAR measurements [*Mastenbroek and de Valk*, 2000].

[11] Another interesting characteristic of the wave measurements used in this work is their geographical location. Right under the line of the Tropic of Capricorn, Campos Basin is strongly affected by swell all the year round with the low-frequency band containing most of the spectral energy measured by the buoy. As pointed out by VMH01, the larger the energy in the part of the spectrum unobserved by SAR, the more difficult the retrieval schemes have in estimating the low-frequency swell. Consequently, one would expect a better performance of the retrieval in this area.

2.2. The WAM Wave Model

[12] In the present study a workstation version of the wave model WAM cycle 4 is run to yield the first guess for the MPI scheme. WAM is a third-generation wave model and has been so far the most validated model running operationally at several forecasting centers (see the WAM Book for more details about the validation exercises and the model characteristics [*Komen et al.*, 1994]). The wave spectra are computed every hour on a latitude-longitude grid with a spatial resolution of 1° covering the whole South Atlantic basin from the equator line to 72°S and from 74°W to 30°E, which totals 7488 grid points. The spectral resolution is 25 frequencies with a logarithmic frequency distribution ranging from 0.042 Hz through 0.41 Hz and 24 directions with a directional resolution of 15°. The wind field at 10 m height used to drive the wave model is from the Atmospheric General Circulation Model (AGCM) which is run by the European Centre for Medium-Range Weather Forecasts (ECMWF). Two data sets are used. The first one is the ECMWF Re-Analysis which comprises the period from 1991 to February 1994, and the second one is the ECMWF Operational Analysis, from March 1994 to December 1995. Both data sets have a latitude-longitude resolution of 1.125°, and the wind field is computed every 6 hours.

[13] The version of the WAM model that runs operationally at the ECMWF has been assimilating significant wave heights obtained from altimeters continuously since August 1993. Since we are also comparing the estimates of the wave model used as first guess to the retrieval against buoy measurements, the possible influence of the assimilation could be assessed using in addition spectra from the ECMWF WAM. However, in our period of interest the only data set including 2D spectra is the ERA (ECMWF Re-analysis), but at the time of development of this work only the year 1993 had been validated

and released. Although the investigation of the influence of the assimilation on the MPI retrievals comparing runs with and without assimilation would be of great value, the use of the results of the WAM model without any sort of modification on the estimates of significant wave height (SWH) has an extra appeal. If one seeks to search for deficiencies in the numerical model through detailed spectral comparisons against buoy measurements, the spurious influence of the assimilation of altimeter data would make the interpretation of the discrepancies more complicated.

2.3. ERS SAR Wave Mode Spectra

[14] SAR is the only instrument so far deployed from satellites that is capable of measuring the full directional wave spectrum and therefore of allowing the complete characterization of a sea state. In SAR image mode the instrument acquires 100 × 100 km images with resolution around 30 × 30 m, but owing to onboard storage limitations, it can be operated only with a ground station in sight. The SAR wave mode (SWM) was introduced to overcome this coverage limitation since the much smaller 10 × 5 km imagettes are stored onboard and transmitted once per orbit to ground stations. With similar resolution to the image mode, SWM are acquired every 30 s yielding an along-track sampling every 200 km and a cross-track spacing of 1000–2000 km with a total of around 1500 images collected every day.

[15] The retrieval of two-dimensional ocean wave spectra from SAR image variance spectra requires the use of inversion schemes which take into account the strongly nonlinear SAR ocean wave imaging process [*Hasselmann and Hasselmann*, 1991]. In order to estimate a complete wave spectrum it is necessary to reverse the distortions caused by motion effects and to blend the SAR measurement with prior information, for example, taken from numerical wave models.

[16] The first algorithm to achieve this was proposed by *Hasselmann et al.* [1996]. The method is based on a two-loop cost function minimization procedure, where the structure of the wave spectrum, i.e., the number and the spectral shape of the different wave systems (partitions), is taken from a prior spectrum. The wavelength, wave height, and wave propagation direction of the partitions are then adjusted iteratively to improve the consistency of SAR measurement and wave spectrum.

[17] A first statistical analysis of the MPI scheme was carried out by *Heimbach et al.* [1998] based on a global data set of 3 years of ERS-1 data. Although this study showed the potential of the SAR data in particular for providing information on longer waves, a rigorous validation with in situ data has not been carried out so far.

[18] It is important to note that the performance of an inversion algorithm depends on both the numerical retrieval procedure and the physical model used to describe the SAR ocean wave imaging process. It is well known that the theoretical imaging model used in the MPI scheme has strong uncertainties in particular with regard to the so-called hydrodynamic modulation mechanism [*Melsheimer et al.*, 1998]. Apart from giving information on ocean wave physics, the analysis presented in this study can also help to improve the understanding of the SAR imaging process and thus to optimize future retrieval methods.

2.4. Collocated Data Sets

[19] A data set was constructed which matches the SAR wave mode acquisitions with the corresponding data available from the wave buoy. The collocation criteria applied to match the data from each source are that the maximum distance between the SWM imagette and the WAM spectrum used as first guess was 50 km and the maximum time separation was 30 min. For the comparison between retrieved wave spectra and buoy measurements the maximum allowed distance and time difference were 150 km and 90 min, respectively, yielding a total of 105 matched spectra evenly spaced over the 1-year period considered. The mean value of SWH of the 105 spectra measured by the buoy is 1.88 m. The ratio between the mean SWH of components longer than 12 s ($H_{S_{12}}$) and mean SWH considering the whole spectral domain (H_{S_t}), that is, $H_{S_{12}}/H_{S_t}$ is equal to 33%, which means that on average around one third of the wave energy is at the low-frequency part of the spectrum. In relation to the satellite track, both paths were equally selected, with 49% of the cases consisting of descending orbit and 51% ascending.

3. Statistical Validation of ERS SAR Retrievals and WAM Estimates Against Buoy Measurements of Significant Wave Height, Propagation Direction, and Mean Frequency

3.1. Methodology

[20] In the work by *Hasselmann et al.* [1996] a partitioning method based on the original idea proposed by *Gerling* [1992] was introduced into the MPI retrieval scheme [*Hasselmann and Hasselmann*, 1991] in an additional iteration loop. In this improved version of the retrieval scheme, after the minimization of the cost function the two-dimensional wave spectrum is divided into different wave systems. Each one of them is represented by a set of mean parameters, that is, significant wave height, propagation direction, and mean frequency. Wave systems from the observed SAR wave spectrum are cross assigned with wave systems from a first guess, and the later iterations are modified to match the mean parameters of the observed wave systems. The result is that the retrieved SAR wave spectrum is smoother in the high wave number cut-off, the region between the observed and non-observed part of the SAR spectrum. In addition, the reduction of the number of spectral values, from 600 bins of 25 frequencies and 24 directions into a number of wave systems, each one represented by some mean parameters, suits very well the requirements of wave data assimilation into models. In the present work the wave systems extracted using the partitioning scheme proposed by *Hasselmann et al.* [1996] are used for the intercomparison.

[21] Different wave systems of different spectra are cross assigned to each other (SAR × Buoy and WAM × Buoy) based on the following criteria.

[22] 1. The coordinates of the two partitions must be within some critical distance to each other in k space. A wave system of a spectrum A with wave numbers (k_x^a, k_y^a) is cross assigned with a wave system of a spectrum B with

wave numbers (k_x^b, k_y^b) if their normalized squared distance in k space is less than some arbitrary value, thus reading

$$\frac{\left(k_x^a - k_x^b\right)^2 + \left(k_y^a - k_y^b\right)^2}{\left(k_x^{a\,2} + k_x^{b\,2}\right) + \left(k_y^{a\,2} + k_y^{b\,2}\right)} \leq 0.75.$$

The arbitrary value of 0.75, the same as suggested by *Hasselmann et al.* [1996], suits well as a first constraint. However, by itself, this criterion is not enough to ensure a reliable match.

[23] 2. In the work by *Hasselmann et al.* [1996], four different classes of wave systems are proposed based on the wave age—wind sea, old wind sea, mixed wind sea–swell, and swell. In the present work, different wave systems are cross assigned if they are of the same type, that is, if both wave systems are pure wind sea (we are not considering old wind sea and mixed wind sea–swell) or both wave systems are swell.

[24] 3. To eliminate spurious partitions the peaks must be above an arbitrary frequency-dependent energy threshold value,

$$e_{\min} = \frac{20 \cdot 10^{-6}}{f_p^4 + 3 \cdot 10^{-3}},$$

where f_p is the peak frequency of the wave system.

[25] 4. If more than one partition fulfills the previous conditions, the closest one is chosen.

[26] Each partition is considered to be an independent wave system generated by different meteorological events and is fully characterized by its significant wave height, mean direction of propagation, and mean frequency. As described by *Hasselmann et al.* [1996] each wave system is defined by an inverted catchment area consisting of spectral points with ascents running into a local peak. Therefore mean parameters can be determined by integrating over the spectral interval (f, θ) to which the partition belongs, defined as follows: (1) Significant wave height (SWH) is $4\sqrt{E_t}$ where E_t is the total energy of a wave system,

$$E_t = \int S(f, \theta)\, df d\theta, \tag{1}$$

(2) mean direction is

$$\arctan\left(\frac{\int S(f,\theta)\sin\theta\, df d\theta}{\int S(f,\theta)\cos\theta\, df d\theta}\right), \tag{2}$$

and (3) mean frequency is

$$\frac{E_t}{\int S(f,\theta) f^{-1}\, df d\theta}. \tag{3}$$

[27] However, the intercomparison of mean parameters based on the cross assignment of different wave systems, each one a component of the full two-dimensional spectrum $S(f, \theta)$, has two drawbacks. In the first place, there is a limitation in the retrieval of the directional spectrum from buoy measurements. From spectral analysis of the three time series acquired by the buoy, that is, the elevation and two orthogonal inclinations in the east and north directions, one can recover the one-dimensional spectrum $S(f)$ and the first four Fourier coefficients, obtained for example from the relations presented by *Long* [1980]. The limitation in the number of coefficients that can be determined is due to the fact that there are only three time series available. The expansion of the spreading function $D(f, \theta)$ as a Fourier series as proposed by *Longuet-Higgins et al.* [1963] is truncated after the second harmonic causing negative lobes, which is not suitable since $D(f, \theta)$ is always positive definite. Other different approaches have been proposed for the representation of the spreading function (and therefore for the reconstruction of the directional spectrum) which can be divided into two main groups, parametric and nonparametric methods. In parametric methods such as those proposed by *Longuet-Higgins et al.* [1963] and *Donelan et al.* [1985], $D(f, \theta)$ has a prescribed form and a controlling parameter which depends on the peak frequency. However, these methods are not consistent when wind sea and swell co-exist in the same frequency band since they tend to fit a single peak in between both wave directions [*Young*, 1994]. In contrast to parametric methods, nonparametric methods such as the Maximum Entropy [*Lygre and Krogstad*, 1986] do not impose any analytical form for the representation of $D(f, \theta)$. In these methods a particular solution from the feasible set of all solutions consistent with the data is selected by minimizing a cost function. However, again owing to the limitation in the number of Fourier components yielded by a heave-pitch-roll buoy, the directional distribution is under-determined, implying that the directional spectra retrieved from buoys have a degree of uncertainty.

[28] In addition to the limitation of single point measurements such as wave buoys for reconstructing the directional spectrum, the use of mean parameters for the intercomparison based only on the cross assignment of wave systems has a second drawback. One of the main difficulties in the cross assignment is the association of a wave system in one spectrum with its counterpart in another spectrum, for example to intercompare the two-dimensional spectrum retrieved from the buoy against the two-dimensional wave spectrum from the model or from SAR. Quite often the SAR wave spectra contain more partitions than the WAM spectra and than the buoy spectra, possibly owing to noise or to limitations in the retrieval scheme [*Hasselmann et al.*, 1996].

[29] Although the criteria listed above seem to be rigorous enough to guarantee the right selection, the cross-assignment procedure may select nonassociated wave systems. Therefore we also apply a second approach where rather than the two-dimensional spectrum the one-dimensional spectrum is used for the intercomparison. From the first Fourier components that are directly measured by the buoy, one can reliably retrieve the one-dimensional energy density spectrum $S(f)$ and some other mean parameters. The two-dimensional directional spectra retrieved from SAR and computed by the WAM are integrated to provide the frequency spectrum $S(f)$ along with the directional distribution and the first

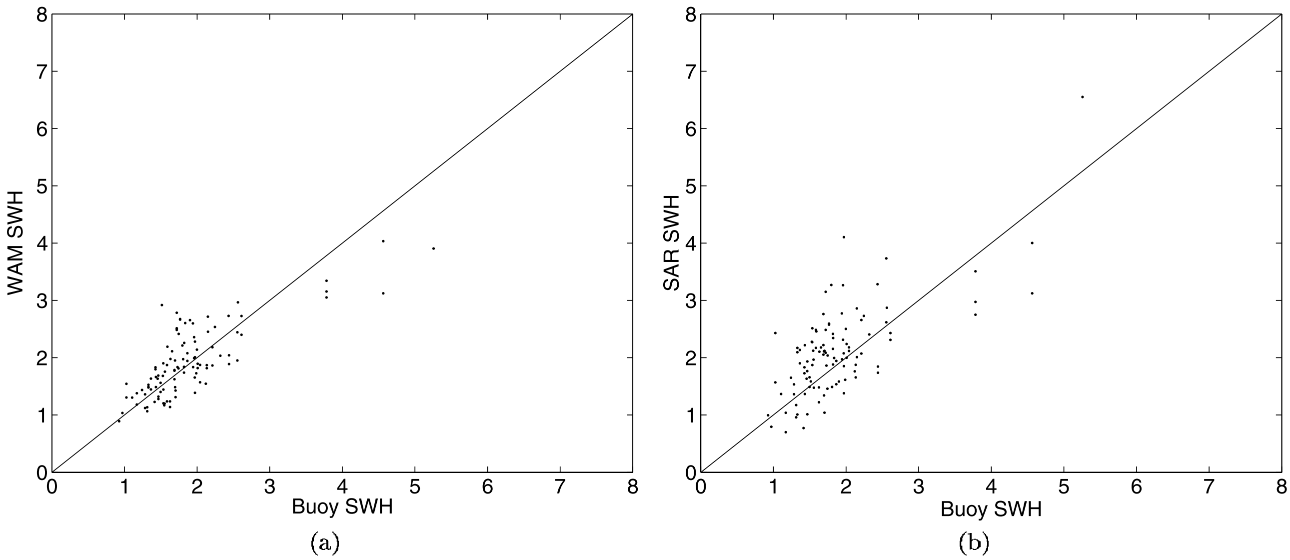

Figure 2. Scatterplots of significant wave height (SWH) calculated using equation (7) and the comparison statistics in Table 1. (a) SWH computed by the WAM model against buoy measurements. (b) SWH retrieved from SAR against buoy measurements. The line of slope unity is also shown.

Fourier coefficients $a_1(f)$ and $b_1(f)$ (see similar approaches in, for example, work of *Voorrips et al.* [1997] and *Wyatt et al.* [1999]). Comparisons are made of parameters over specific frequency bands: 4 s to 6 s, 6 s to 8 s, and so on up to 16 s to 18 s. The mean parameters over specific frequency bands are calculated as follows (using the method presented by *Kuik et al.* [1988]): (1) SWH is $4\sqrt{e_t}$ where e_t is the total energy over the frequency band from $f_{\min}$ till $f_{\max}$,

$$e_t = \int_{f_{\min}}^{f_{\max}} S(f)df, \tag{4}$$

(2) mean direction is

$$\arctan\left(\frac{b_1(f)}{a_1(f)}\right), \tag{5}$$

and (3) mean frequency is

$$\frac{e_t}{\int_{f_{\min}}^{f_{\max}} S(f)f^{-1}df}. \tag{6}$$

Naturally $f_{\max}$ and $f_{\min}$ delimit the frequency band interval, and the Fourier coefficients $a_1(f)$ and $b_1(f)$ are also calculated over the same interval. The main advantage of this second approach is that no type of directional distribution is imposed and the mean parameters, including direction of propagation and directional spread, are determined directly by the first Fourier coefficients. Moreover, the intercomparison is performed using specific frequency bands rather than individual wave systems which will ensure that only related information will be intercompared.

[30] Although the intercomparison of the one-dimensional spectra over specific frequency bands seems to be more rigorous than the cross assignment of partitioned wave systems, both approaches will be presented and discussed in the following. Wave systems from the partitioning scheme have been used so far in some assimilation exercises [*Hasselmann et al.*, 1997; *Dunlap et al.*, 1998] and in another intercomparison study [*Heimbach et al.*, 1998]. For assimilation purposes the use of individual partitions seems to be the most operationally feasible solution. However, as commented earlier, the cross assignment of wave systems is subject to a degree of uncertainty that, at best, needs to be investigated. There is a trade-off between being sufficiently rigorous to ensure the correct selection and the need to avoid imposing excessive constraints and therefore unreasonably reducing the number of matches.

3.2. Significant Wave Height

[31] In order to validate the performance of the MPI retrieval scheme and the WAM model against buoy measurements, we calculate the energy of all wave components integrating over the whole frequency domain, as in

$$H_{S_t} = 4\left\{\int S(f)df\right\}^{1/2}. \tag{7}$$

The scatterplots of significant wave height of SAR and WAM against buoy measurements are shown in Figure 2, and their statistics are compared in Table 1. The performance of the wave model is superior to the SAR, in terms of bias, standard deviation, and normalized RMS error. Although the MPI scheme uses the WAM spectra as first guess to the inversion, the results of SWH retrieved from SAR are worse. The scatter in the WAM is about 25% lower than the scatter in the SAR retrievals, with the MPI scheme adding its own error. The same was observed in VMH01, but in that work the correlation between both WAM-Buoy and SAR-Buoy was higher, probably because they have selected a narrower collocation window (maximum time and distance of 30 min and 80 km between SAR and buoy measurements) and owing to the fact that altimeter data have been assimilated into the ECMWF WAM model

Table 1. Statistics of the Comparisons Against Buoy Measurements of Significant Wave Height (SWH) Calculated Using Equation (7)[a]

	Points	Bias	St Dev	NRMSE	corr
WAM	105	0.04	0.44	0.22	0.79
SAR	105	0.22	0.59	0.31	0.71

[a]Statistics include bias, standard deviation (St Dev), RMS error normalized with the RMS buoy wave height (NRMSE), and correlation (corr).

used in their comparison. However, the values of normalized RMS error that we find are very similar to the ones obtained by VMH01. In our results the mean value of SWH retrieved by the MPI scheme is 9.6% higher than the mean value of SWH computed by the WAM, which is consistent with the results reported by *Dunlap et al.* [1998].

[32] In the imaging of wind waves by SAR the radial velocity of the sea surface caused by the orbital motions of the waves results in an azimuthal displacement due to the Doppler effect of a moving target. As a consequence, there is a loss of information in the azimuth direction beyond a high wave number cut-off. This cut-off wave number is sea state dependent, but in general, waves shorter than 150/200 m propagating parallel to the satellite track are not mapped directly by SAR. In the MPI scheme in general a wave model is used as a first guess to augment the spectral information beyond the cut-off and to resolve the directional ambiguity inherent in frozen images. Therefore, to investigate the performance of the MPI scheme in the low wave number band where waves are mapped directly onto the SAR image, we calculate the energy of the wave components longer than 225 m (or periods longer than 12 s in deep water),

$$H_{S_{12}} = 4\left\{\int_{f_1}^{f_2} S(f)df\right\}^{1/2}, \tag{8}$$

where $f_1 = 0$ and $f_2 = 1/12$ Hz.

[33] The scatterplots of the low wave number wave heights using equation (8) are shown in Figure 3 and the comparison statistics in Table 2. In contrast to the results presented in Figure 2 and Table 1, the performance of the MPI retrieval scheme is as good as the WAM model for values of significant wave height in the low-frequency band of the spectrum. Apart from the fact that the WAM results are virtually bias free, the MPI retrievals have a standard deviation and a normalized RMS error of the same order as the WAM. These results are in contrast with those presented in VMH01, where the WAM results compare slightly better with buoy measurements than the MPI retrievals, even considering only the low-frequency part of the spectrum.

[34] There are two main differences between our comparisons and the ones presented by VMH01, the collocation criteria and the wave model used as first guess to the inversion. In VMH01 a narrower collocation window, both in time and space, was imposed which to some extent would explain their greater correlation when considering the energy of the spectrum over the whole frequency interval using equation (7). In VMH01, most of the buoys are located in relatively shallow waters where one would expect a greater variability of the wave parameters when compared to the more spatially homogeneous situations encountered by the deep water buoy in Campos Basin. However, when considering the frequency band directly mapped onto SAR images (equation (8)), our results are very similar to the ones presented in VMH01, which indicates that our coarser collocation criteria is not the cause for the discrepancy.

[35] The second main difference between the present study and VMH01 is that although both use the spectra calculated by the WAM model as first guess to the inversion, in VMH01, altimeter data have been assimilated into the ECMWF WAM version. In this paper, no assimilation was used in the model forecasts, and the spectra computed by the WAM are the direct result of the physics behind the

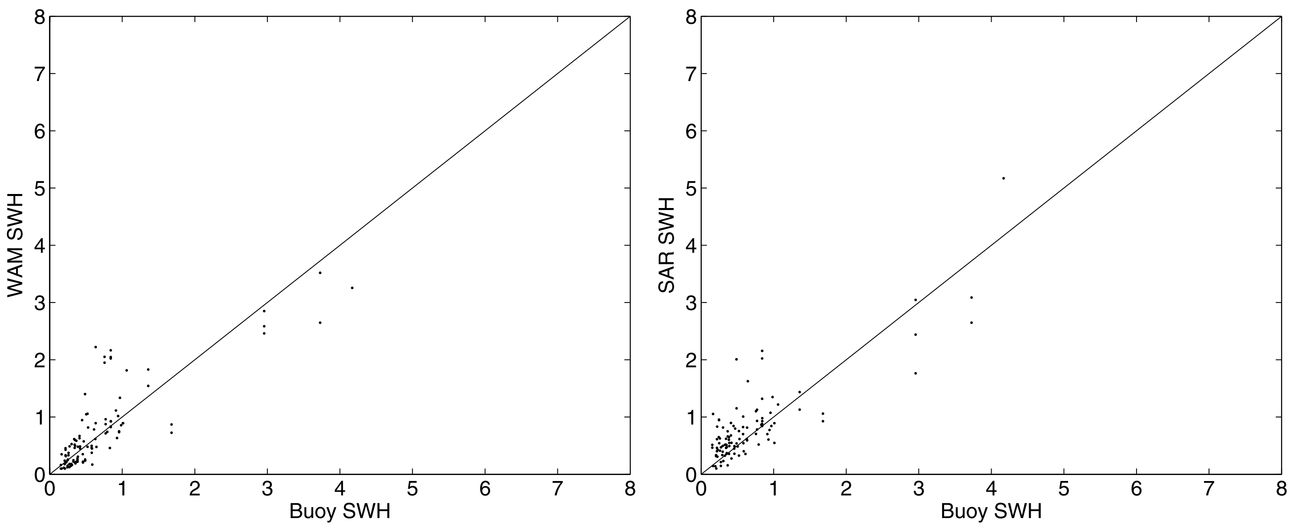

(a) (b)

Figure 3. Same as Figure 2 but for values of $H_{S_{12}}$ (equation (8)) and the comparison statistics in Table 2. The mean value of SWH measured by the buoy is 0.70 m.

Table 2. Statistics of the Comparisons Against Buoy Measurements of Significant Wave Height (SWH) Calculated Using Equation (8)[a]

	Points	Bias	St Dev	NRMSE	Corr
WAM	105	0.05	0.42	0.41	0.84
SAR	105	0.13	0.41	0.41	0.85

[a]Statistics include bias, standard deviation (St Dev), RMS error normalized with the RMS buoy wave height (NRMSE), and correlation (corr).

model. If assimilation of altimeter data is in fact the reason for the somewhat better performance of the WAM results compared with the MPI retrievals in the low-frequency part of the spectrum as presented in VMH01, then this fact raises an interesting point about their conclusions. The main conclusion in the work by VMH01 is that the MPI retrieval scheme deteriorates the quality of the first guess used by the inversion. At first, this seems to be corroborated by our results shown in Figure 2, when the high wave number band is considered in the calculation of SWH. However, Figure 3 shows that the low wave number SWH retrieved from the MPI scheme does not in fact degrade the low wave number SWH estimated by the model and used as first guess.

[36] One of the main characteristics of the MPI retrieval scheme is the partitioning method discussed above which isolates and cross assigns different wave systems from the inverted SAR wave spectrum and the WAM first guess spectrum. As a result, at the end of the retrieval, not only has the directional SAR wave spectrum been recovered, but each wave system is defined by a number of mean parameters as well. The reduction of the number of degrees of freedom of the wave spectrum is a very desirable feature that has been exploited in data assimilation studies. Figure 4 and Table 3 show the scatterplots of SWH for the cross assignment of partitions using equation (1). The reason why the number of partitions that were cross assigned differ among plots (and are different from the number of spectra in Figures 2 and 3) is that more than one partition per spectrum might be selected. The statistics in Table 3 are similar to those in Table 1, which indicates that the criteria for the cross assignment listed at the beginning of this section are rigorous enough to ensure that only related partitions will be selected. The statistics of the wave systems whose mean wavelength are greater than 225 m (crosses in Figure 4) would give us insights about the performance of the retrieval of long waves. However, the low number of points that resulted from applying this constraint, 29 and 26, respectively, for SAR and WAM is too small to be statistically meaningful.

[37] In order to analyze the SWH retrieved from SAR and estimated by the model in more spectral detail, we calculate the energy of the wave components over specific frequency bands using equation (4). The results are shown in Figure 5. *Heimbach et al.* [1998] compared WAM estimates against SAR retrievals that used the wave model results themselves as first guess. They found a systematic underprediction of the energy of the swell components and an overprediction of the wind sea, whereas from our measurements this trend was not observed. The WAM estimates are virtually bias free whereas the MPI retrievals show a positive bias over the whole spectral range. It is worth mentioning, however, that for periods smaller than approximately 12 s the information retrieved from the MPI scheme derives from the WAM model and therefore the retrieval is adding its own error, increasing the bias. However, in the part of the spectrum directly observed by SAR (periods greater than 12 s) the bias of the MPI

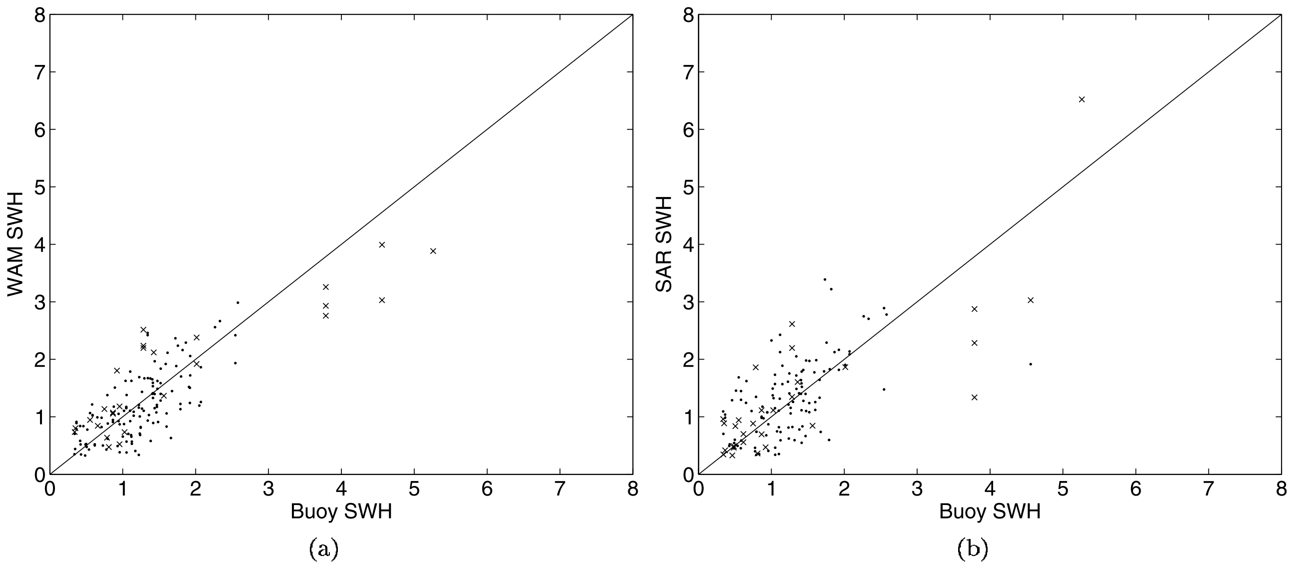

Figure 4. Scatterplots of SWH for every partition calculated using equation (1) and the comparison statistics in Table 3 with the line of slope unity drawn passing through the origin. (a) SWH computed by the WAM model against buoy measurements and with mean value of SWH measured by the buoy equal to 1.31 m. (b) SWH retrieved from SAR against buoy measurements and with mean value of SWH measured by the buoy equal to 1.28 m. The crosses are the partitions whose mean wavelength are greater than 225 m: periods greater than 12 s.

Table 3. Statistics of the Comparisons Against Buoy Measurements of Significant Wave Height (SWH) Calculated Using Equation (1)[a]

	Points	Bias	St Dev	NRMSE	Corr
WAM	156	−0.02	0.48	0.31	0.80
SAR	143	0.05	0.64	0.42	0.69

[a]Statistics include bias, standard deviation (St Dev), RMS error normalized with the RMS buoy wave height (NRMSE), and correlation (corr).

scheme gradually decreases with wave period, and for very long waves (periods longer than 16 s) it performs better than the model with a smaller bias. The standard deviation and the normalized RMS error of both the MPI retrievals and the model estimates show a trend to increase with period, the MPI scheme presenting greater errors for waves with periods smaller than 12 s. Likewise the error of the MPI scheme in the low wave number part of the spectrum is of the same order as (and for longer wavelengths even smaller than) the WAM results.

3.3. Propagation Direction

[38] The waves measured by the buoy have two characteristic features: relatively short waves with a westward component and a northward long swell generated far away from Campos Basin. Since the ERS satellite had a polar orbit, the long northward swell is propagating in the azimuth direction and the shorter westward waves travel in the range direction. In Figure 6 we present a comparison between the different results for the histograms of the direction of propagation of the wave systems calculated using equation (2). The statistics of the point by point comparisons are presented in Table 4. The overall statistics of the WAM-Buoy comparison appears to be better than the SAR-Buoy with smaller errors and a greater correlation. However from the point by point comparison shown in Table 4 it is not clear whether the wave model and the retrieval perform better for longer or shorter wave systems. In Figure 6 it is clear that the agreement of the SAR-Buoy comparison is much better in the northward and northwestward direction of propagation; that is, the results of the MPI retrievals compare better with the buoy data for long swell.

[39] Figure 7 shows the results from calculating the propagation direction using equation (5). The WAM results present a very small bias for waves with periods shorter than 10 s, but for longer waves the bias has a trend to increase with wave period. In the part of the spectrum observed by SAR (waves with periods longer than 12 s) the MPI retrievals have a slightly smaller bias than WAM. Both WAM estimates and the MPI retrievals have a directional resolution of 15° which is of the same order as the maximum bias found. The standard deviation and the normalized RMS error of both WAM and MPI directions increase with wave period.

3.4. Mean Frequency

[40] We present in Figure 8 histograms of mean frequency of retrieved SAR and WAM estimates against buoy measurements using (3), and their statistics are presented in Table 5. Similar to the results of propagation direction, the overall

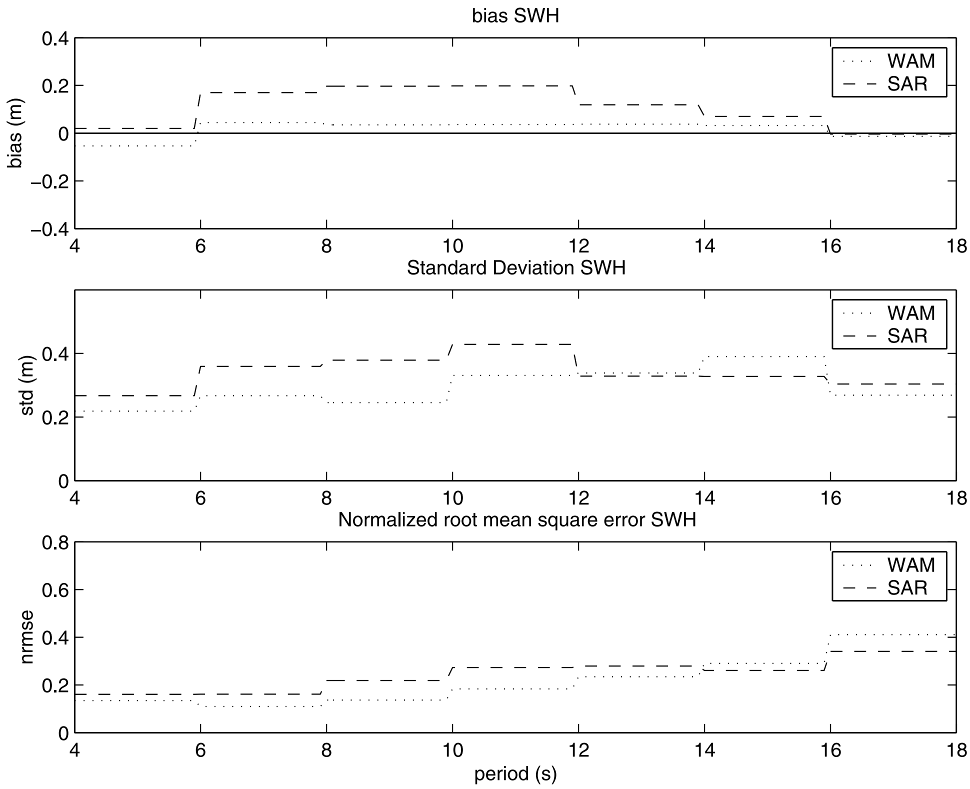

Figure 5. Statistics of SWH compared with buoy measurements over frequency bands using equation (4).

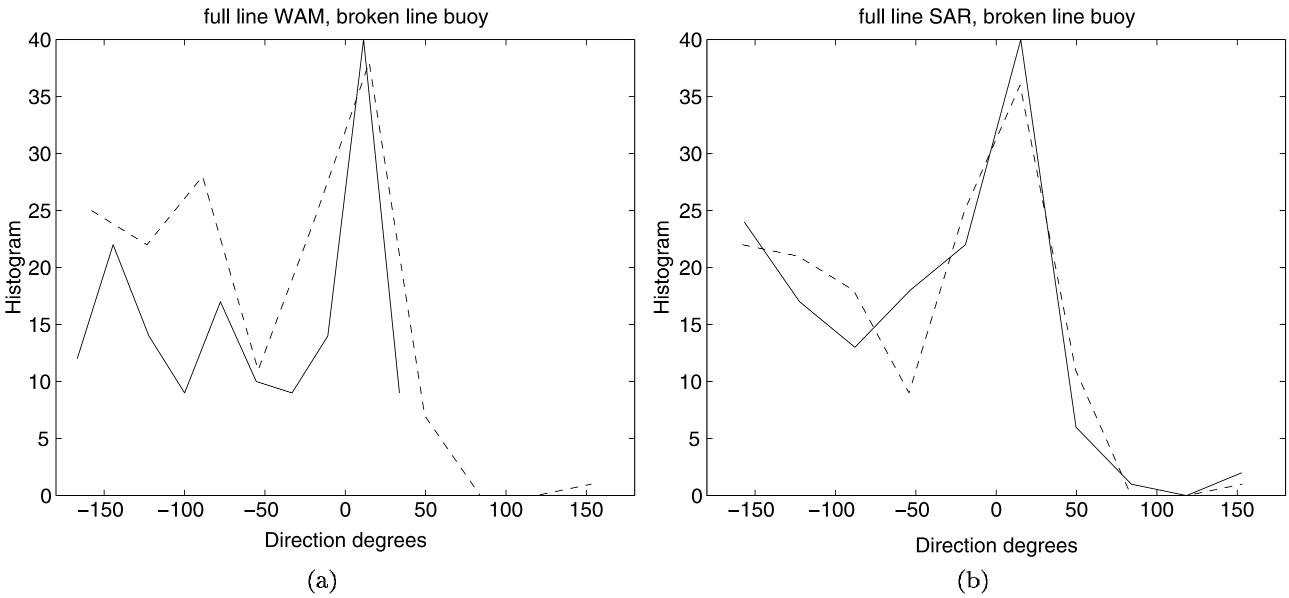

Figure 6. Histograms of the mean direction of propagation (direction waves go to) of (a) the WAM estimates and buoy measurements and (b) the MPI retrievals and buoy measurements. Buoy measurements are represented by the dashed lines, whereas the MPI and WAM are represented by the solid lines.

statistics of the wave model are superior to the SAR results although once again the plots should be examined carefully for the spectral detail. The comparison of WAM results against buoy data shows two distinct regimes; the high-frequency band has a much better agreement than the low-frequency part of the spectrum. This is in contrast with the SAR-Buoy comparison where for longer waves the MPI retrievals compare better with buoy measurements than the model results.

[41] Figure 9 shows that both the MPI scheme and the WAM model tend to underestimate the mean frequency of short waves. Both WAM and SAR show a negative bias in frequency for periods shorter than 12 s and a trend to decrease with wave period, whereas for longer waves the bias shows the opposite trend. Standard deviation and normalized RMS for both WAM and SAR decrease with wave period. The standard deviation in the band of periods from 4 to 8 s is 5 times larger than for periods greater than 16 s. Both in terms of bias and error the MPI retrievals perform better than WAM estimates for waves with periods longer than 12 s.

4. Underestimation of the Mean Frequency of Short Waves by the WAM Model

[42] The larger errors encountered in the band of short wave components in Figure 9 could be explained by a wrong wind input used by the WAM where the negative bias would be related to an overestimation of modeled wind speeds. Owing to the sparseness of observations, especially at sea, the deficiencies of meteorological models in computing the wind in the Southern Hemisphere are well known. The selection of about 100 cases of wind measurements acquired by the offshore buoy, distributed over the whole year of analysis, yielded a good opportunity to also validate the wind fields estimated by the ECMWF model. Figure 10 is a point by point comparison of the wind speeds measured by the buoy and the wind speeds calculated by the ECMWF atmospheric model. The overall agreement is good, with a correlation coefficient of 0.70 and normalized root mean squared (rms) error of 36%. The spread is relatively high, with a standard deviation of the order of 50% of the mean buoy wind speed. The bias of the model wind speed is low, about 6% of the mean value measured by the buoy, and its negative value represents an underestimation of the modeled wind speed. Consequently, it seems that the wind input is not the cause for the poorer agreement in the high-frequency band.

[43] The underestimation of the mean frequencies calculated by the WAM could be related to the spectral discretization employed. One of the main features of second-generation wave models is that to ensure a stable spectral evolution, some sort of parameterization is imposed, in general with some prescribed spectral form being applied to the wind sea [*SWAMP Group*, 1985]. A third-generation wave model such as WAM, on the other hand, computes the wave spectrum integrating the energy balance equation without any restriction on the spectral shape [*Komen et al.*, 1994; *Young*, 1999]. The fundamental role of the nonlinear interactions in the growth of wind waves became clear

Table 4. Statistics of the Comparisons Against Buoy Measurements of the Direction of Propagation of the Wave Systems Calculated Using Equation (2)[a]

	Points	Bias	St Dev	NRMSE	Corr
WAM	156	0.93	33.50	0.37	0.88
SAR	143	4.84	53.10	0.60	0.72

[a]Statistics include bias, standard deviation (St Dev), RMS error normalized with the RMS buoy wave height (NRMSE), and correlation (corr). Bias and standard deviation are in degrees.

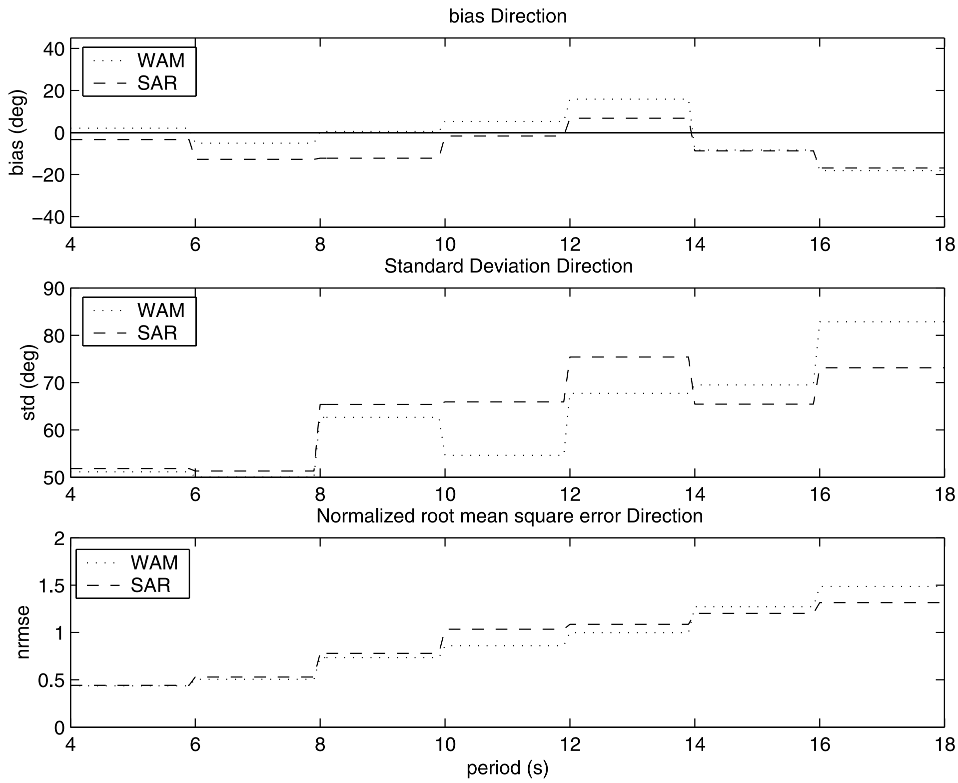

Figure 7. Values of direction of propagation over frequency bands using equation (5).

during the JONSWAP experiment [*Hasselmann et al.*, 1973]. In the initial growth phases of fetch or duration-limited wind seas a peak normally starts to develop at high frequencies just after the wind begins to blow. The nonlinear interactions cause a migration of energy from higher frequencies to frequencies near the spectral peak. The nonlinear interactions are also responsible for a spectral shape stabilization, forcing the high-frequency portion of the spectrum to decay in a manner inversely proportional to frequency [*Young and van Vledder*, 1993]. The result is that as the wind continues to blow, the spectrum broadens and the peak shifts to lower frequencies with increasing fetch up to the point where it attains full development.

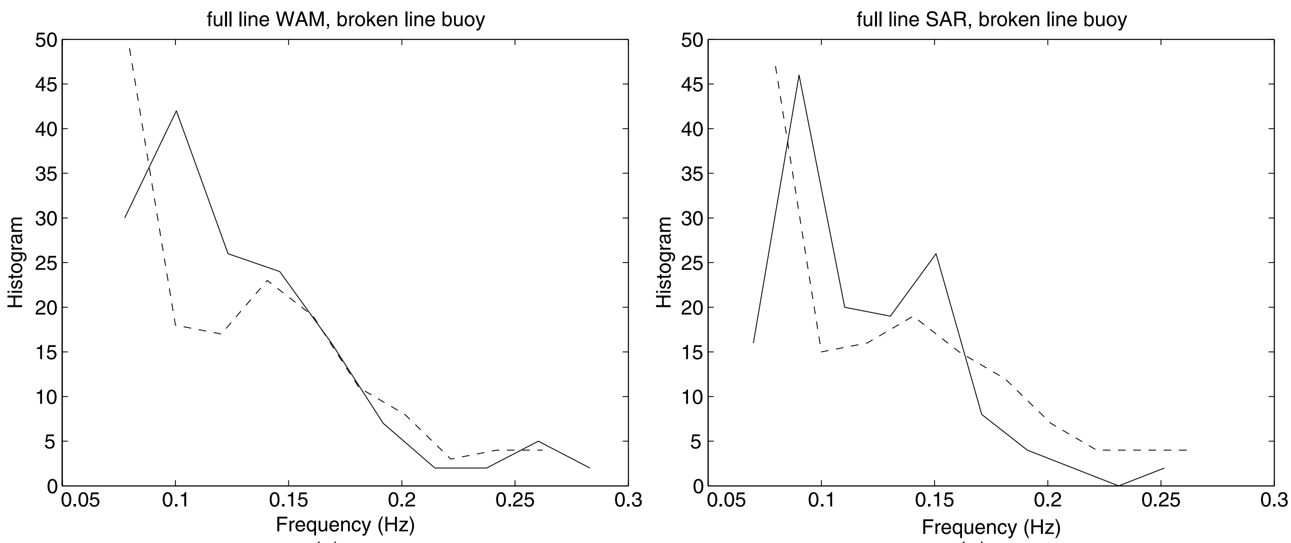

(a) (b)

Figure 8. Histograms of the mean frequency of (a) the WAM estimates and buoy measurements and (b) the MPI retrievals and buoy measurements. Buoy measurements are represented by the dashed lines, whereas the MPI and WAM are represented by the solid lines. Mean frequency is calculated using (3).

Table 5. Statistics of the Comparisons Against Buoy Measurements of the Mean Frequencies of the Wave Systems Calculated Using Equation (3)[a]

	Points	Bias	St Dev	NRMSE	Corr
WAM	156	−0.0017	0.0299	0.21	0.82
SAR	143	−0.0131	0.0354	0.27	0.73

[a]Statistics include bias, standard deviation (St Dev), RMS error normalized with the RMS buoy wave height (NRMSE), and correlation (corr). Bias and standard deviation are in Hertz.

[44] Hence the proper estimation of the wave spectrum by a third-generation model in the initial phases of growth is closely connected to the frequency discretization used for high frequencies. Beyond the maximum high frequency used in the model the wind sea growth cannot be simulated properly since the transfer of energy from higher frequencies through nonlinear interactions will be neglected. Around the cut-off frequency the wind sea peak starts to grow slowly only because of the direct input of energy by the wind. Only after it attains a higher spectral level do the nonlinear interactions then begin to act and the peak gradually migrates to lower frequencies. Thus the choice of the highest discrete frequency is fundamental for the modeling of the wind wave development since it will impose the initial position of the peak in frequency space and in addition will determine the time interval necessary for the nonlinear interactions to become effective.

[45] The spectral discretization used in the present version of the WAM cycle 4 is 24 directions and 25 logarithmically spaced frequencies from 0.042 Hz to 0.41 Hz [*WAMDI Group*, 1988]. *Tolman* [1992] has investigated numerical errors in third-generation wave models and their influence on the initial stages of growth. Considering scaling laws, and the effect of the frequency range for different wind speeds, Tolman concludes that the frequency discretization used in the WAM produces good scaling behavior for wind speeds of 15 to 25 m/s whereas for lower winds the mean wave energy is overestimated and the mean frequency is underestimated. This optimal wind speed range is high, particularly considering tropical regions where lower wind speeds are much more common. Using 10 years of wind measurements acquired on an oil platform in Campos Basin, *Violante-Carvalho et al.* [1997] describe typical meteorological situations encountered in the study area, where 97% of the wind speeds observed during this period are below 15 m/s and 74% are below 9 m/s. Thus, clearly, the mean wind speeds in Campos Basin are lower than the optimal range for applying the model frequency discretization.

[46] The underestimation of the mean frequency by the WAM in the early stages of wave growth as observed in Figure 9 could be related to the diagnostic tail added beyond a high-frequency cut-off. The wave spectrum estimated by the model consists of a prognostic part which extends up to 2.5 times the mean frequency (or maximally up to 0.41 Hz) and beyond this point a diagnostic part represented by an f^{-4} tail. Therefore beyond 0.41 Hz the model cannot simulate properly the initial growth of the wind sea since the modeled waves develop near the cut-off only in response to the wind input rather than by nonlinear transfer of energy from higher frequencies. Since the nonlinear transfer is only triggered after a certain level, this results in a delay in the

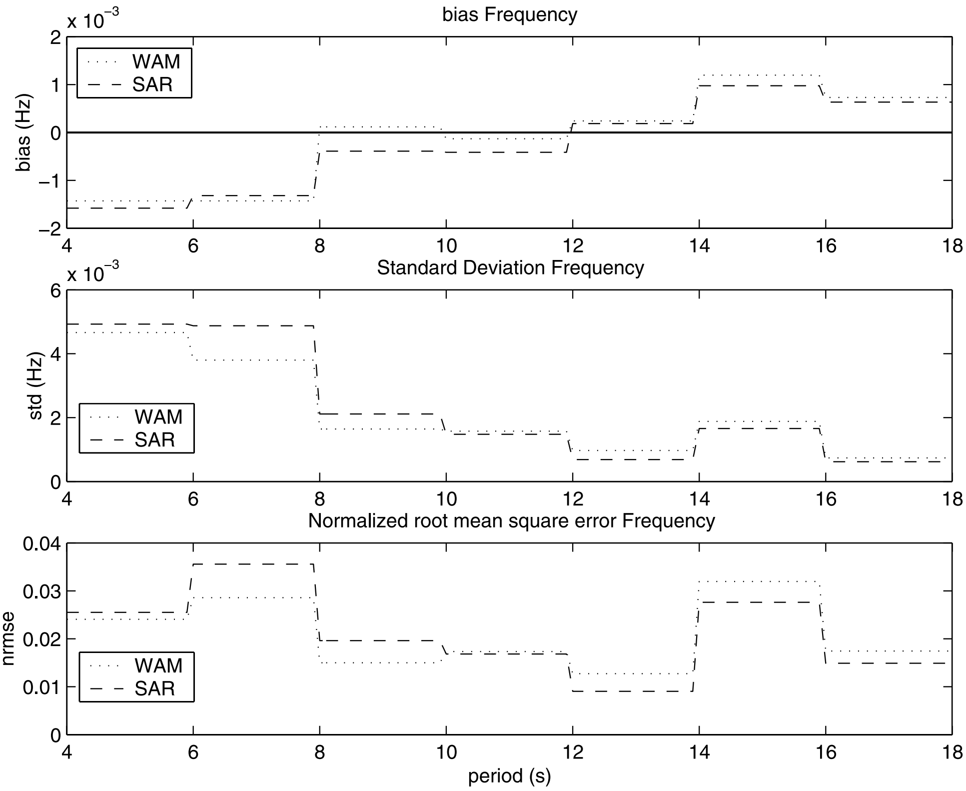

Figure 9. Values of the mean frequency over frequency bands using equation (6).

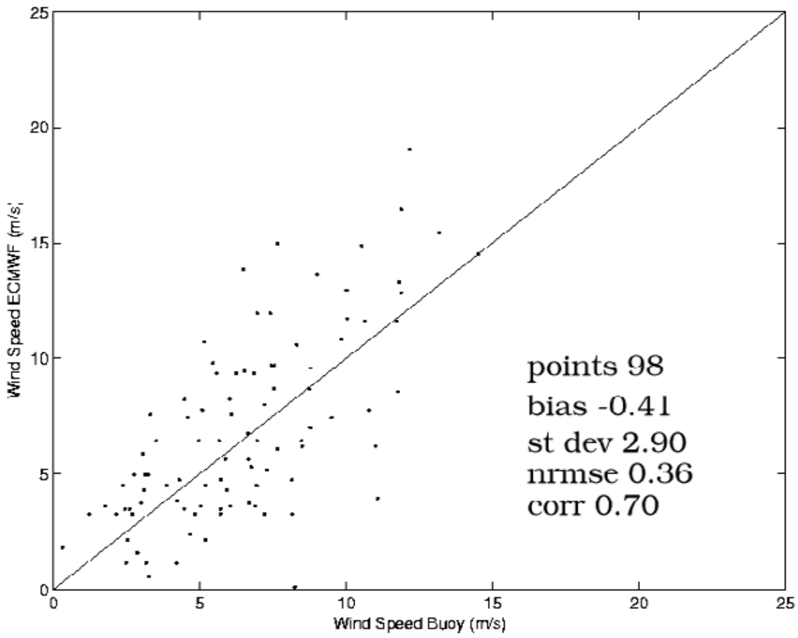

Figure 10. Scatterplot of the wind speed measured by the buoy and estimated by the ECMWF model (in m/s for a reference height of 10 m). The comparison statistics are also shown: respectively, bias, standard deviation (st dev), RMS error normalized with the RMS buoy wind speed (nrmse), and correlation (corr). The mean wind speed measured by the buoy is 6.5 m/s.

development of the wind sea peak which, in addition, is located at lower frequencies.

[47] *Tolman* [1992] also shows the effect of the extension of the high-frequency cut-off to a much higher value of 0.97 Hz and as a result the reduction of the discrepancies with wave energies and mean frequencies closer to non-dimensional growth curves. This underestimation of the mean frequency of the wind sea in early stages of development is more easily detectable through detailed spectral comparisons like the one presented in Figure 9. When the mean frequency is calculated over the whole spectral domain or comparisons are performed on a global scale, as most of the validation tests of the WAM have been so far, this limitation of the model in the initial generation phases is less likely to be found.

5. Comparisons of Directional Wave Spectra

5.1. The Directional Spreading Retrieved From the MPI Scheme

[48] The overall performance of the MPI retrievals is best measured by quantitative matchup statistics such as those obtained above, although direct comparisons of the directional spectra are interesting to enable a clearer understanding of the differences through qualitative validations. We are, however, comparing spectra obtained in rather different ways. Remote sensing instruments like ERS SAR measure the wave number spectrum whereas the wave model WAM estimates the frequency spectrum. The buoy, on the other hand, yielded the frequency spectrum $S(f)$ from the heave series and the first Fourier coefficients, the directional distribution being reconstructed using the Maximum Entropy Method [*Lygre and Krogstad*, 1986]. One way to assess the differences among spectra is to determine the Fourier coefficients by integrating the directional spectra and to compare them with the coefficients measured directly by the buoy.

[49] In the MPI scheme the WAM first guess wave systems are rotated and scaled in order to adjust to the wave systems of the inverted SAR wave spectrum. However, their spectral forms are not allowed to vary, which means that the spectral widths of the wave systems retrieved from the MPI scheme are the same as those from the first guess wave model. The importance of the nonlinear term S_{nl} in determining the directional spreading has been pointed out by *Donelan et al.* [1985] and later confirmed by numerical simulations of *Banner and Young* [1994] and evidence from measurements [*Young et al.*, 1995]. In third-generation wave models the directional spreading is computed from the integration of the source terms where S_{nl} forces the spectrum to a typical shape with a relatively narrow spread around the peak that slowly broadens at higher and lower frequencies [*Young and van Vledder*, 1993]. The directional distribution predicted by the model used by *Banner and Young* [1994], however, employed the full solution of the nonlinear source term called Exact-NL. In the WAM model the complex wave-wave nonlinear interaction term S_{nl} is approximated by a non-exact solution called the DIA (Discrete Interaction Approximation) for computational efficiency. Although the SWH computed from the WAM model has been exhaustively tested against measurements, the impact of the DIA on the spreading has not yet been quantitatively demonstrated.

[50] In order to assess the performance of the MPI scheme in estimating the directional spreading we present in Figure 11 a swell component propagating in the azimuth direction with its frequency spectrum and directional

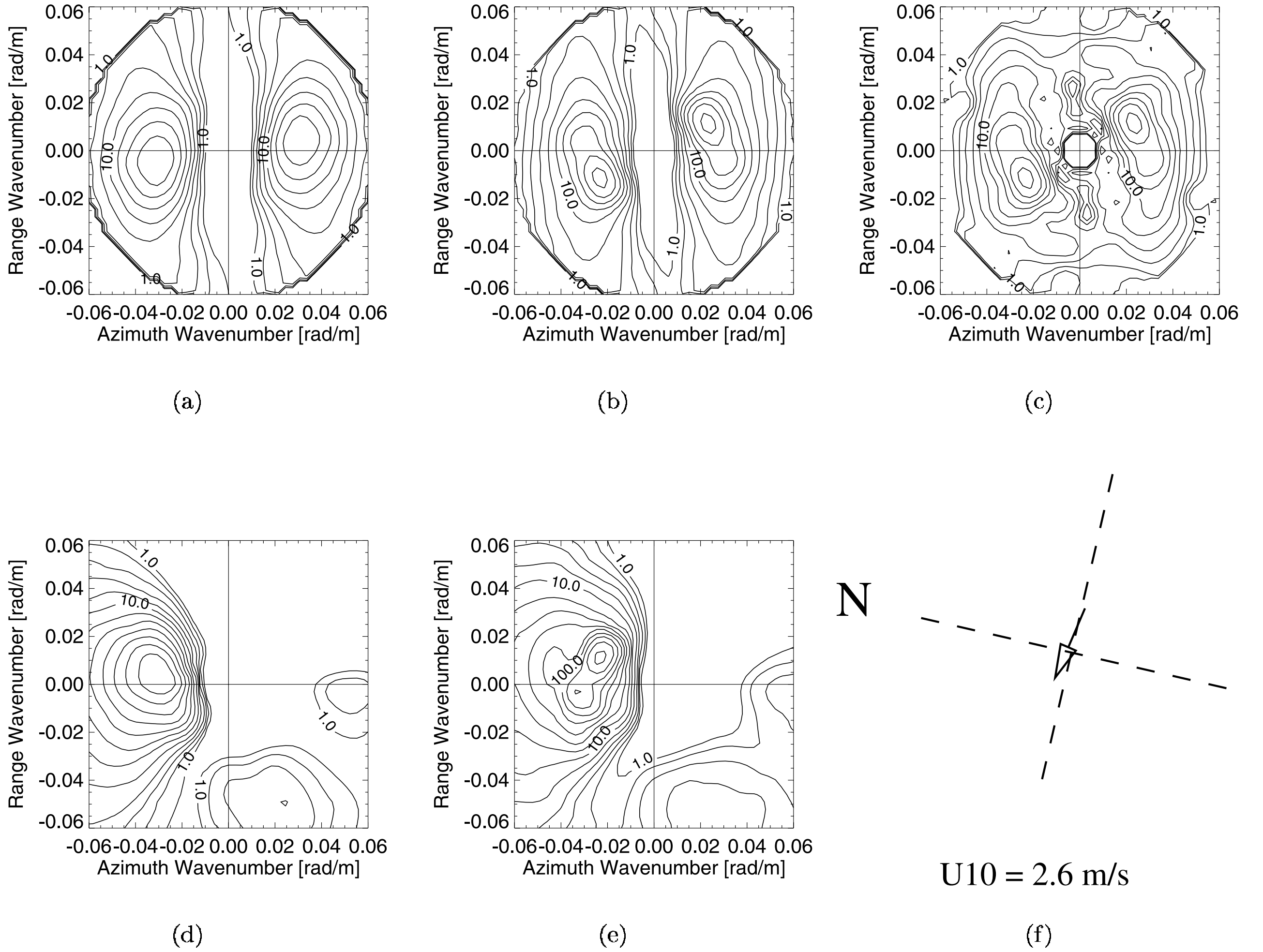

Figure 11. Example of a 195-m swell on 29 August 1994, 1243 UT. The top row shows SAR image spectra, and the bottom row shows wave spectra (with the exception of the right panel). (a) WAM image spectrum, (b) the image spectrum retrieved by the MPI scheme, and (c) the observed SAR spectrum. (d) WAM wave spectrum and (e) the wave spectrum retrieved by the MPI scheme. (f) Arrow indicates the wind speed estimated by the model (no wind information available from the buoy).

spreading shown in Figure 12. The spreading is calculated using the expression proposed by *Kuik et al.* [1988],

$$\sigma(f) = \left(2\left(1 - \sqrt{a_1^2(f) + b_1^2(f)}\right)\right)^{\frac{1}{2}}, \qquad (9)$$

where $a_1(f)$ and $b_1(f)$ are the first Fourier coefficients. The overall agreement of the directional spectra is good (compare Figures 11d, 11e, and 12a) although the model overestimates the wind sea component in the range direction. In Figure 12b the input wave spectrum from the WAM slightly underestimates the value of SWH measured by the buoy with a somewhat broader angular distribution. As shown in VMH01, since the MPI scheme is not allowed to narrow the spectrum width, it has no choice other than increasing the energy level.

[51] The values of $\sigma(f)$ are presented in Figure 12c, where the directional spectra of the SAR retrievals and WAM estimates are integrated to provide the Fourier coefficients. The values of $\sigma(f)$ computed from the coefficients directly measured by the heave-pitch-roll buoy (Buoy Coef in Figure 12c) are also shown, with the typical shape of a narrow distribution around the peak that broadens at both higher and lower frequencies. The directional spreading computed by the model and retrieved from SAR presents much the same value of directional spread at the peak of the spectrum, which is narrower than the one calculated from the Fourier coefficients measured by the buoy.

[52] Another case, in which there is a very long and energetic swell component generated far away from Campos Basin and a SWH measured by the buoy of 8.9 m, is illustrated in Figures 13 and 14. Once again, the agreement between spectra is good (Figures 1d, 13e, and 14a) in terms of frequency, direction, spreading and energy. In Figure 14c the same behavior of the spreading as in the previous case is observed. From the two examples shown, a northward swell and a much longer and more energetic case, it may be concluded that the spreading computed from the model (and therefore imposed on the spectrum retrieved by the MPI scheme) seems to represent fairly well the spreading directly computed from the buoy data. Although the value at the peak is slightly narrower, the overall shape of the directional spread retrieved by the MPI scheme describes

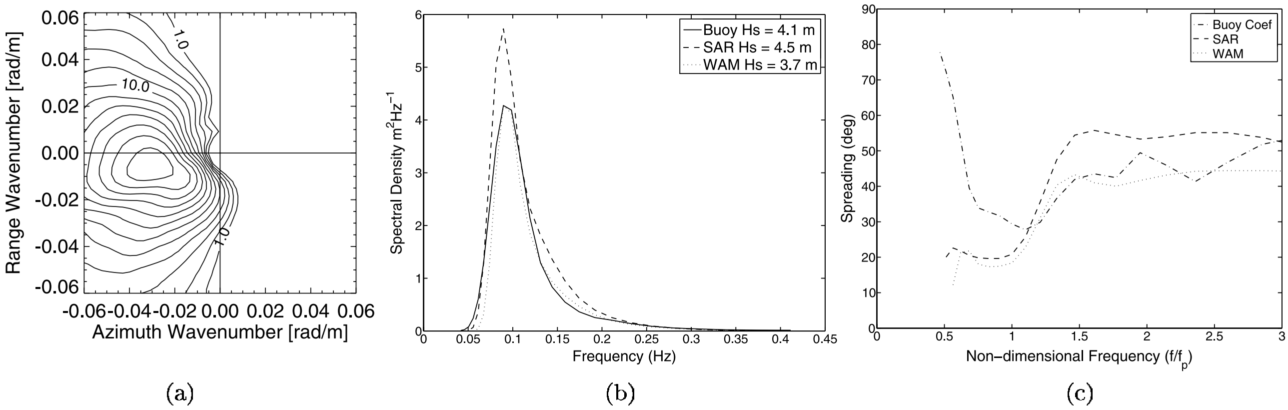

Figure 12. (a) Wave spectrum measured by the buoy for the case in Figure 11. (b) Frequency spectrum with the values of significant wave height. (c) Spreading function calculated using equation (9) directly calculated from the Fourier coefficients (Buoy Coef), and from the SAR and WAM.

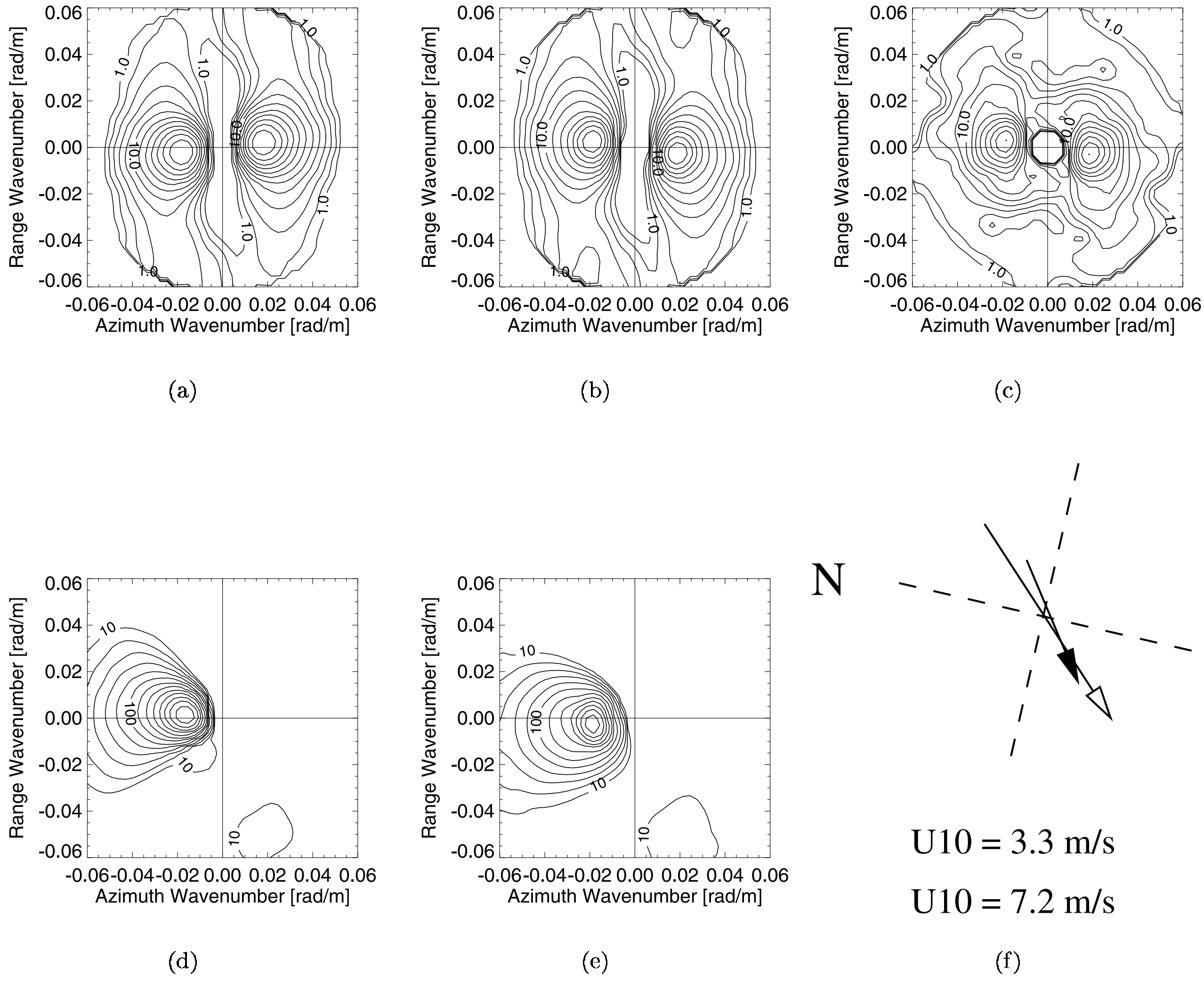

Figure 13. Example of a 345-m swell propagating northward (in azimuth direction) on 30 June 1994, 1250 UT. (a) WAM image spectrum, (b) the image spectrum retrieved by the MPI scheme, and (c) the observed SAR spectrum. (d) WAM wave spectrum and (e) the wave spectrum retrieved by the MPI scheme. (f) Wind speed measured by the buoy is indicated by the black arrow (first value of U10 on top), and the wind speed estimated by the ECMWF model is indicated by the open arrow (second value of U10).

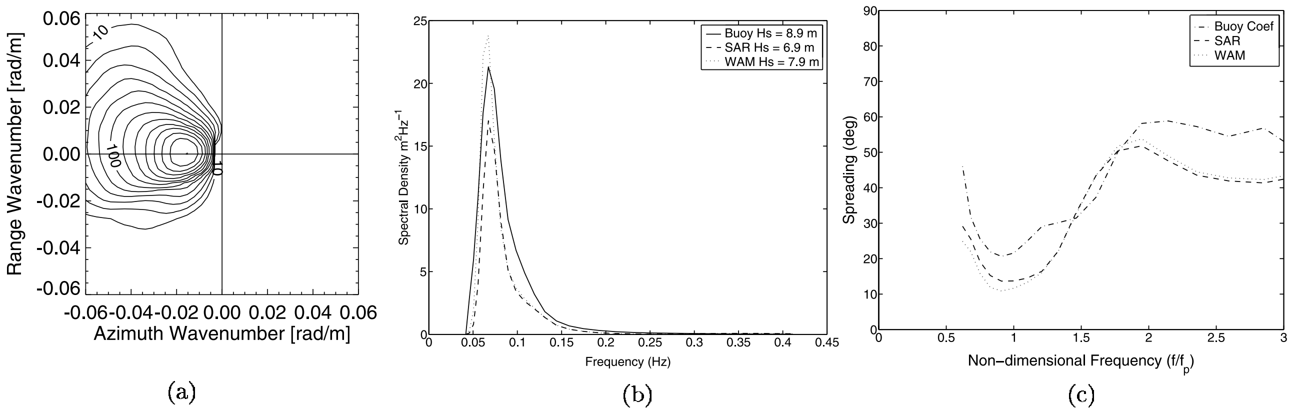

Figure 14. Directional spectrum measured by the buoy, frequency spectrum, and spreading for the same case in Figure 13.

very well the same trend measured by the buoy in the selected cases.

5.2. Nonlinearities in the SAR Imaging Mechanism

[53] Nonlinear SAR degradation of azimuth waves causes energy of high wave number waves to be transferred to low azimuthal wave numbers. In the MPI scheme, for computational reasons, the SAR spectrum is mapped back to the wave spectrum using a quasi-linear approximation to the mapping relations, in contrast to the forward mapping that uses the full nonlinear transform [*Hasselmann and Hasselmann*, 1991]. The quasi-linear term is an approximation to the full nonlinear transform obtained by terminating the expansion after the first linear terms where the azimuthal cut-off is retained. *Mastenbroek and de Valk* [2000] and VMH01 have already discussed the implications of neglecting the transfer of energy when the quasi-linear approximation is employed, resulting in the generation of spurious swell peaks in the azimuth direction.

[54] Figures 15 and 16 show the case of a swell peak erroneously enhanced by this effect. The frequency spectrum (Figure 16b) illustrates a poor first guess where the wind sea component is underestimated by the WAM model probably because of an underestimation of the wind input by the ECMWF model (Figure 15f). The energy that this wind sea creates in low azimuth wave number through the nonlinearities in the SAR mapping mechanisms is erroneously interpreted by the MPI scheme as swell, which was already overestimated by the WAM model. The result is a swell peak that is 10 times larger than the one measured by the buoy. It is worth noting that although the value of SWH computed by the model is exactly the same as the one measured by the buoy, the frequency spectra differ enormously, which demonstrates the need for detailed spectral information in assimilation exercises.

[55] When the directional spectrum measured by the buoy in the case illustrated in Figure 15 is used as first guess to the inversion, the retrieved wave spectrum is that presented in Figure 16c. The spurious peak at low frequency has disappeared, and although the wind sea is somewhat underestimated, the swell component is well retrieved in terms of direction, frequency, energy and directional spread (Figures 15d and 15e). This case demonstrates how the nonlinearities in the SAR imaging mechanisms may be erroneously interpreted by the MPI scheme, causing wind sea energy to be transferred to low azimuth wave numbers.

6. Discussion

[56] One year of measurements acquired in tropical deep waters in the South Atlantic is employed to perform intercomparisons of wave spectra retrieved by the MPI scheme and estimated by the WAM model. For the first time, a scheme for the retrieval of wave spectra from ERS SAR images was statistically validated against directional buoy observations. Two different approaches were applied. In the first, wave systems extracted from a partitioning method of the directional spectrum are cross assigned and their main parameters, that is SWH, mean direction, and mean frequency, are intervalidated. The comparison of wave systems, each one a constituent of the directional spectrum, is of interest for being an operationally feasible option for wave data assimilation studies. In the second approach, the directional spectra retrieved from SAR images and estimated by the model are integrated to provide the frequency spectrum. The comparisons of the main wave parameters are made over specific frequency bands, which ensures that only related information is being assessed. The statistics of SWH obtained using both approaches are very similar, which is indicative of the suitability of the criteria employed for the cross assignment.

[57] In a previous validation exercise where only SWH was taken into account, VMH01 concluded that the MPI scheme increases the bias and the error of the WAM spectra used as first guess, even considering only the low wave number part of the spectrum directly mapped onto SAR images. Confirming partially their findings, we have observed that the MPI scheme degrades the values of SWH used as first guess for the inversion. The scatter in the WAM-Buoy point by point comparisons of SWH is 25% lower than the SAR-Buoy scatter, indicating that the MPI scheme adds its own error. The mean value of SWH retrieved by the MPI scheme is about 10% higher than the mean value of SWH estimated by the model, which is consistent with the results presented by *Dunlap et al.* [1998]. However, in contrast to the findings presented in VMH01, we have found that the performance of the MPI scheme, when only the low wave number part of the

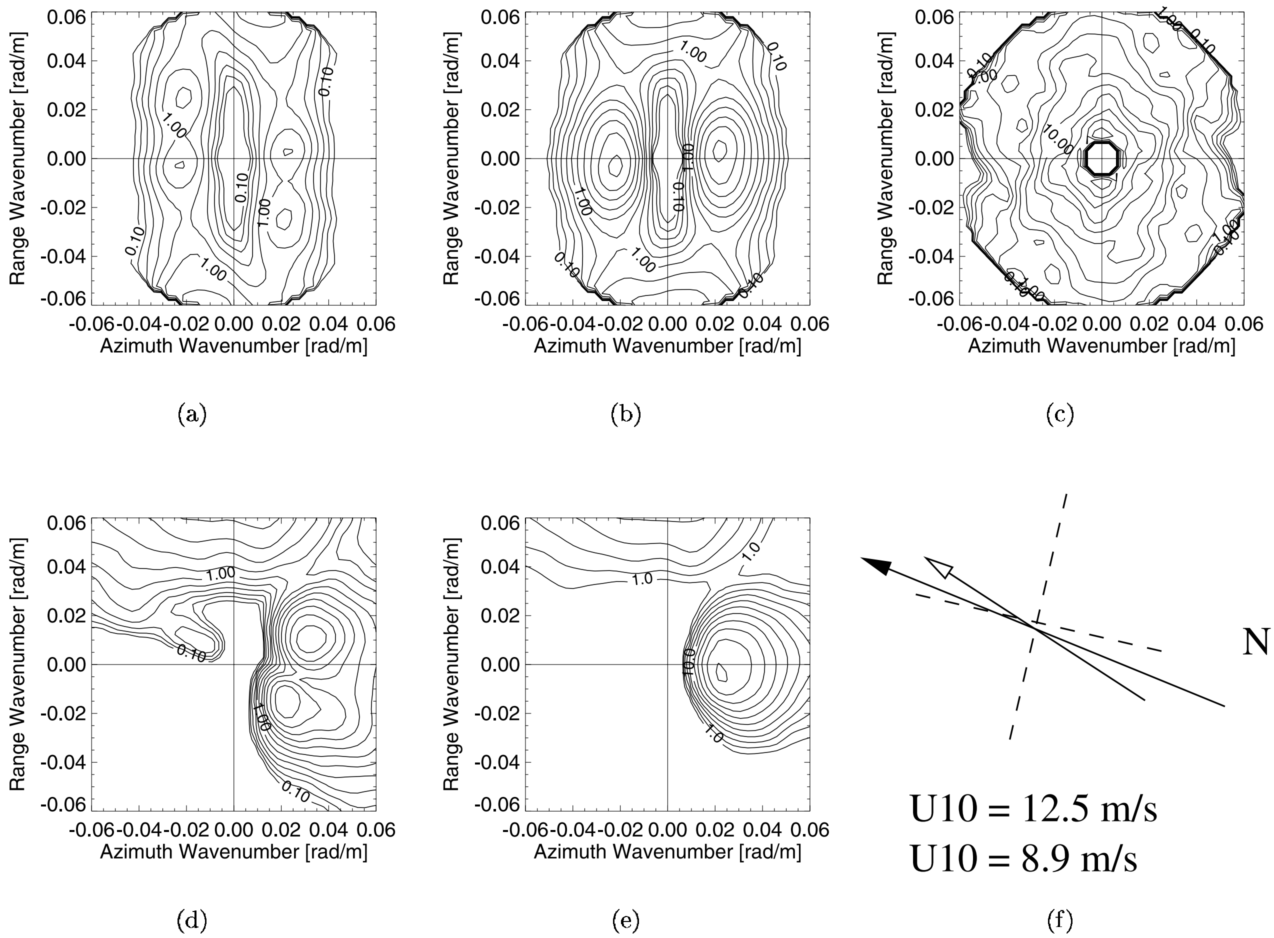

Figure 15. An erroneously enhanced swell peak due to a poor first guess on 28 November 1994, 0141 UT. The top row shows SAR image spectra, and the bottom row shows wave spectra (with the exception of the right panel). (a) WAM image spectrum, (b) the image spectrum retrieved by the MPI scheme, and (c) the observed SAR spectrum. (d) WAM wave spectrum and (e) the wave spectrum retrieved by the MPI scheme. (f) Arrows indicate the wind speed estimated by the model. The wind speed measured by the buoy is indicated by the black arrow (first value on top), and the wind speed estimated by the ECMWF model is indicated by the open arrow (second value of U10).

spectrum (waves longer than 225 m) is included in the computation of SWH, is at least as good as the wave model. The main difference between both studies is the WAM model employed. The ECMWF WAM version used in VMH01 has assimilated SWH from altimeter data whereas our first-guess wave spectra were estimated without any type of assimilation procedure.

[58] As well as the assessment of SWH, directional wave parameters were also considered in our analysis. For short waves the MPI scheme also degrades the retrievals of mean direction of propagation and mean frequency, where the model spectra used as first guess compare better to the buoy spectra than the retrievals. However, for waves longer than 225 m, directly measured by SAR, the performance of the MPI scheme is at least as good as the WAM model. However, most of the long wave energy is in the 12–14 second band, so any conclusions drawn need to bear in mind that the results in the wave period bands longer than 14 s are not particularly relevant. In addition to the shortcomings of the algorithm to extend the spectral information beyond the high wave number cut-off, another constraint is the way that the MPI scheme deals with the nonlinearities in the SAR imaging mechanism. The use of the quasi-linear model to map the SAR image spectrum back to the wave spectrum might cause the algorithm to interpret a transfer of wind sea energy to low azimuth wave number components as swell.

[59] Some discrepancies have been identified between the mean frequency of short waves estimated by the model and measured by the buoy. The underestimation of the computed mean frequencies may be explained by an inadequate spectral discretization employed by the model, which appears to cause a delay in the development of the wind sea peak. WAM and SAR retrievals perform better for longer waves, with both bias and error decreasing slowly with wave period.

[60] The retrieval of the directional spreading was assessed through some selected qualitative validations. In the MPI scheme the spectral shapes of the retrieved wave systems are the same as their counterparts in the WAM first guess wave spectrum. The spreading computed by a third-generation wave model depends on the integration of the

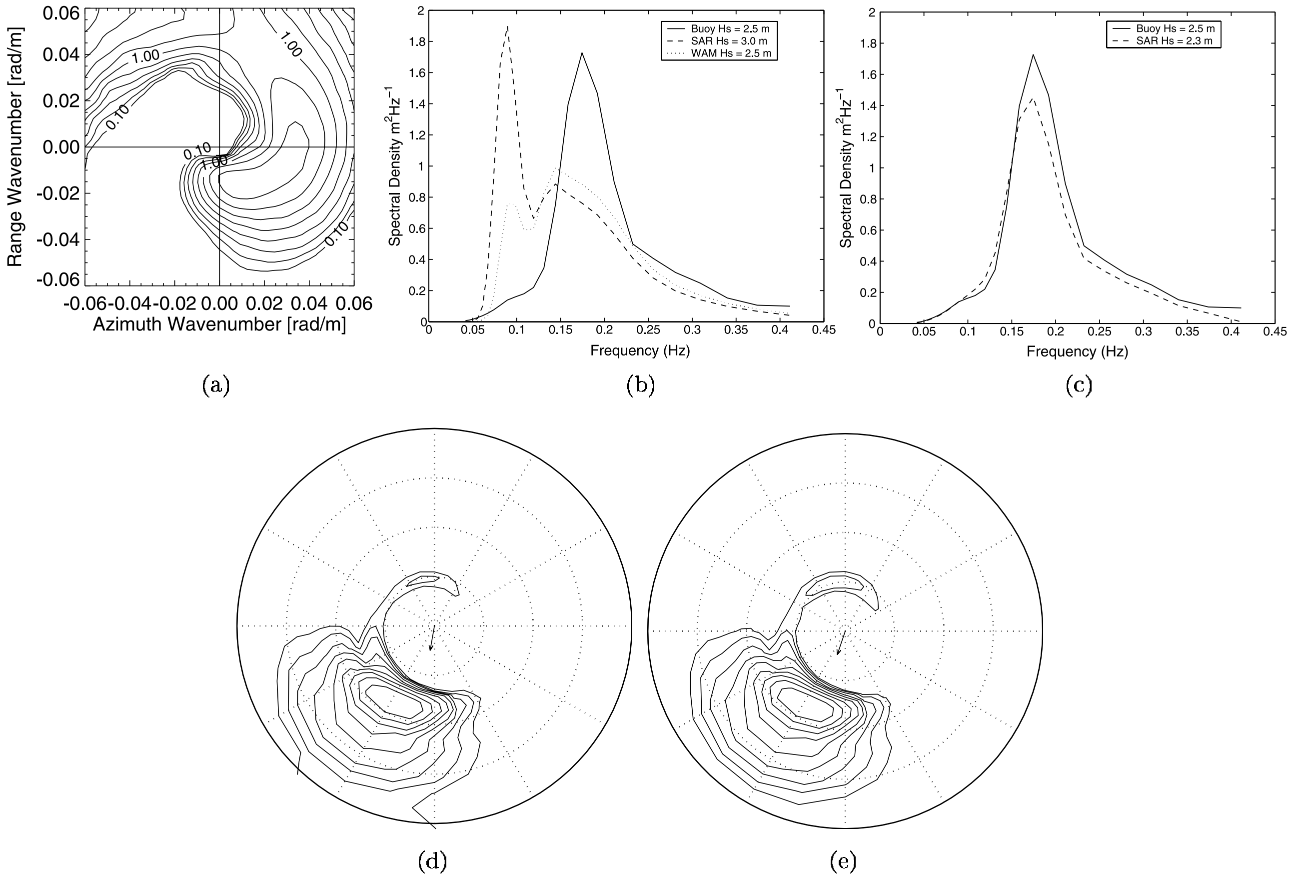

Figure 16. (a) Directional spectrum measured by the buoy and (b) frequency spectrum, for the same case as in Figure 15. (c) Frequency spectrum retrieved using the directional spectrum measured by the buoy as first guess to the inversion. (d) Directional spectrum of the buoy measurement and (e) the retrieved SAR wave spectrum correspondent to Figure 16c with both spectra in polar frequency-directional plots with the wind direction represented by the arrow in the center. Circles denote frequency at 0.1 Hz interval from 0.1 Hz (inner circle) to 0.4 Hz (outer circle). Isolines are logarithmically spaced relative to the maximum value of the spectral energy density.

source terms, whereas the nonlinear interactions S_{nl} play a key role in this process as has already been demonstrated by simulations and in situ measurements [*Donelan et al.*, 1985; *Young and van Vledder*, 1993; *Banner and Young*, 1994]. The impact on the directional spread of the non-exact approximation of the calculation of S_{nl}, called discrete interaction approximation (DIA), has not yet been quantitatively demonstrated. However, there is considerable uncertainty associated with the spread retrieved from heave-pitch-roll buoys due to the limitation in the number of time series acquired by the instrument, which means that the buoy in this case is not a reliable reference for the other observations. Hence a cross-validation exercise was performed, where the spread retrieved by the MPI scheme (and therefore estimated by the model) and computed from the Fourier Coefficients directly measured by the buoy were compared. The MPI and WAM results are very close to the value computed from the Fourier coefficients. However, a statistical validation of the retrieved spreading against the values obtained by the heave-pitch-roll buoy has not yet been performed. One of the main reasons for such a lack of this type of statistical validation is the complicated shape of the directional spreading when peaks lie close to one another in frequency space. A possible way forward for investigating the spreading could be a spectral approach based on the partitioning of the directional spectrum, where different wave systems are classified in accordance with their mean direction, energy, frequency, and spreading. Once different wave systems are correctly cross assigned, their respective Fourier coefficients could yield valuable information about their different spreading characteristics, an approach that should be pursued in further work.

[61] In summary, our study, the first to use open ocean directional wave buoy data to validate SAR-derived spectra, confirms that the MPI scheme indeed degenerates the high wave number part of the first-guess spectrum increasing the bias and the error of the wave parameters, that is SWH, mean direction of propagation, and mean frequency. However, for longer swell components it does not make the input spectrum any worse. On the contrary, its performance is at least as good as the WAM wave model, and therefore what this paper shows is not that SAR has no value in improving wave spectra, but that it cannot at present improve on the WAM forecasts, except possibly at the lowest frequencies. However, given the small number

of sample points in bands longer than 14 s, these results should not be considered as definitive, although they do point out the importance of making further validation studies using directional wave buoy measurements from deep ocean locations.

[62] **Acknowledgments.** We are grateful to PETROBRAS, the Brazilian Oil Company, for making available the buoy data. Violante-Carvalho has been supported by the Brazilian research funding agency CNPq. Violante-Carvalho also acknowledges the support of the European COST714 Action, who sponsored the period that he spent as a Visiting Researcher working with Susanne Lehner at the German Space Agency (DLR) in Oberpfaffenhofen, Germany. The help of L. R. Wyatt and M. Srokosz in discussing an early draft of this paper is greatly appreciated.

References

Banner, M. L., and I. R. Young (1994), Modeling spectral dissipation in the evolution of wind waves: Part I. Assessment of existing model performance, *J. Phys. Oceanogr.*, *24*, 1550–1571.

Bauer, E., K. Hasselmann, I. R. Young, and S. Hasselmann (1996), Assimilation of wave data into the wave model WAM using an impulse response function method, *J. Geophys. Res.*, *101*(C2), 3801–3816.

de las Heras, M., G. Burgers, and P. A. E. M. Janssen (1994), Variational wave data assimilation in a third-generation wave model, *J. Atmos. Oceanic Technol.*, *11*, 1350–1369.

Donelan, M. A., J. Hamilton, and W. H. Hui (1985), Directional spectra of wind-generated waves, *Philos. Trans. R. Soc. London, Ser. A*, *315*, 509–562.

Dunlap, E. M., R. B. Olsen, L. Wilson, S. D. Margerie, and R. Lalbeharry (1998), The effect of assimilating ERS-1 fast delivery wave data into the North Atlantic WAM model, *J. Geophys. Res.*, *103*(C4), 7901–7915.

Gerling, T. (1992), Partitioning sequences and arrays of directional ocean wave spectra into component wave systems, *J. Atmos. Oceanic Technol.*, *9*, 444–458.

Hasselmann, K., and S. Hasselmann (1991), On the nonlinear mapping of an ocean wave spectrum into a Synthetic Aperture Radar image spectrum and its inversion, *J. Geophys. Res.*, *96*(C6), 10,713–10,729.

Hasselmann, K., et al. (1973), Measurements of wind-wave growth and swell decay during the Joint North Sea Wave Project (JONSWAP), *Dtsch. Hydrogr. Z. Suppl.*, *A8*(12), 95 pp.

Hasselmann, K., P. Lionello, and S. Hasselmann (1997), An optimal interpolation scheme for the assimilation of spectral wave data, *J. Geophys. Res.*, *102*(C7), 15,823–15,836.

Hasselmann, S., C. Brüning, K. Hasselmann, and P. Heimbach (1996), An improved algorithm for the retrieval of ocean wave spectra from Synthetic Aperture Radar image spectra, *J. Geophys. Res.*, *101*(C7), 16,615–16,629.

Heimbach, P., S. Hasselmann, and K. Hasselmann (1998), Statistical analysis and intercomparison of WAM model data with global ERS-1 SAR wave mode spectral retrievals over 3 years, *J. Geophys. Res.*, *103*(C4), 7931–7977.

Komen, G. J., L. Cavaleri, M. A. Donelan, K. Hasselmann, S. Hasselmann, and P. A. E. M. Janssen (1994), *Dynamics and Modelling of Ocean Waves*, 532 pp., Cambridge Univ. Press, New York.

Krogstad, H. E., O. Samset, and P. W. Vachon (1994), Generalizations of the non-linear ocean-SAR transform and a simplified SAR inversion algorithm, *Atmos. Ocean*, *32*(1), 61–82.

Kuik, A. J., G. P. van Vledder, and L. H. Holthuijsen (1988), A method for the routine analysis of pitch-and-roll buoy wave data, *J. Phys. Oceanogr.*, *18*, 1020–1034.

Lionello, P., H. Günter, and P. A. E. M. Janssen (1992), Assimilation of altimeter data in a global third-generation wave model, *J. Geophys. Res.*, *97*(C9), 14,463–14,474.

Long, R. B. (1980), The statistical evaluation of directional spectrum estimates derived from pitch/roll buoy data, *J. Phys. Oceanogr.*, *10*, 944–952.

Longuet-Higgins, M., D. Cartwright, and N. Smith (1963), Observations of the directional spectrum of sea waves using the motion of a floating buoy, in *Ocean Wave Spectra*, pp. 111–136, Prentice-Hall, Upper Saddle River, N. J.

Lygre, A., and H. E. Krogstad (1986), Maximum entropy estimation of the directional distribution in ocean wave spectra, *J. Phys. Oceanogr.*, *16*, 2052–2060.

Mastenbroek, C., and C. F. de Valk (2000), A semiparametric algorithm to retrieve ocean wave spectra from Synthetic Aperture Radar, *J. Geophys. Res.*, *105*(C2), 3497–3516.

Melsheimer, C., M. Bao, and W. Alpers (1998), Imaging of ocean waves on both sides of an atmospheric front by the SIR-C/X-SAR multifrequency synthetic aperture radar, *J. Geophys. Res.*, *103*(C9), 18,839–18,849.

SWAMP Group (1985), *Ocean Wave Modeling*, 256 pp., Springer, New York.

Tolman, H. L. (1992), Effects of numerics on the physics in a third-generation wind-wave model, *J. Phys. Oceanogr.*, *21*, 1095–1111.

Violante-Carvalho, N., and I. S. Robinson (2004), On the retrieval of two dimensional directional wave spectra from spaceborne Synthetic Aperture Radar (SAR) images, *Sci. Mar.*, *68*(3), 317–330.

Violante-Carvalho, N., L. M. P. Nunes, and W. Tavares Jr. (1997), Typical conditions and extreme values of wind speed in Campos Basin, *Tech. Rep. 005/97*, PETROBRAS, Rio de Janeiro.

Violante-Carvalho, N., F. J. Ocampo-Torres, and I. S. Robinson (2004), Buoy observations of the influence of swell on wind waves in the open ocean, *Appl. Ocean Res.*, *26*(1–2), 49–60.

Voorrips, A. C., V. K. Makin, and S. Hasselmann (1997), Assimilation of wave spectra from pitch-and-roll buoys in a North Sea wave model, *J. Geophys. Res.*, *102*(C3), 5829–5849.

Voorrips, A. C., A. W. Heemink, and G. J. Komen (1999), Wave data assimilation with the Kalman filter, *J. Mar. Syst.*, *19*, 267–291.

Voorrips, A. C., C. Mastenbroek, and B. Hansen (2001), Validation of two algorithms to retrieve ocean wave spectra from ERS Synthetic Aperture Radar, *J. Geophys. Res.*, *106*(C8), 16,825–16,840.

WAMDI Group (1988), The WAM model—A third generation ocean wave prediction model, *J. Phys. Oceanogr.*, *18*, 1775–1810.

Wyatt, L. R., S. P. Thompson, and R. Burton (1999), Evaluation of high frequency radar wave measurements, *Coastal Eng.*, *37*, 259–282.

Young, I. R. (1994), On the measurement of directional wave spectra, *Appl. Ocean Res.*, *16*, 283–294.

Young, I. R. (1999), *Wind Generated Ocean Waves*, 288 pp., Elsevier, New York.

Young, I. R., and G. P. van Vledder (1993), A review of the central role of nonlinear interactions in wind-wave evolution, *Philos. Trans. R. Soc. London, Ser. A*, *342*, 505–524.

Young, I. R., L. A. Verhagen, and M. L. Banner (1995), A note on the bimodal directional spreading of fetch-limited wind waves, *J. Geophys. Res.*, *100*(C1), 773–778.

I. S. Robinson, Southampton Oceanography Centre, University of Southampton, European Way, Southampton SO14 3ZH, UK. (isr@soc.soton.ac.uk)

J. Schulz-Stellenfleth, Institut für Methodik der Fernerkundung, DLR, D-82234 Wessling, Germany. (johannes.schulz-stellenfleth@dlr.de)

N. Violante-Carvalho, Department of Oceanography, Rio de Janeiro State University, Rua S/ao Francisco Xavier 524, Rio de Janeiro 20550-013, Brazil. (violante_carvalho@yahoo.co.uk)